JGR Atmospheres

RESEARCH ARTICLE
10.1029/2020JD033989

The Impact of Split and Displacement Sudden Stratospheric Warmings on the Troposphere

Ian P. White[1], Chaim I. Garfinkel[1], Judah Cohen[2,3], Martin Jucker[4], and Jian Rao[1]

[1]The Hebrew University of Jerusalem, Institute of Earth Sciences, Jerusalem, Israel, [2]Atmospheric and Environmental Research Inc., Lexington, MA, USA, [3]Massachusetts Institute of Technology, Cambridge, MA, USA, [4]Climate Change Research Centre, University of New South Wales, Sydney, NSW, Australia

Key Points:

- Little difference in the longer-term (3–4 weeks+) surface response in either free-running or thermally forced displacement and split events
- Conversely, large differences are apparent between displacements and splits at shorter lags
- Displacements yield stronger stratospheric temperature anomalies than splits yet still give rise to similar-magnitude tropospheric responses

Supporting Information:

Supporting Information may be found in the online version of this article.

Correspondence to:

I. P. White,
ian.white@mail.huji.ac.il

Citation:

White, I. P., Garfinkel, C. I., Cohen, J., Jucker, M., & Rao, J. (2021). The impact of split and displacement sudden stratospheric warmings on the troposphere. *Journal of Geophysical Research: Atmospheres*, *126*, e2020JD033989. https://doi.org/10.1029/2020JD033989

Received 13 DEC 2020
Accepted 24 MAR 2021

Abstract Although sudden stratospheric warmings (SSWs) can improve subseasonal-to-seasonal forecasts, it is unclear whether the two types of SSW - displacements and splits - have different near-surface effects. To examine the longer-term (i.e., multi-week lead) tropospheric response to displacements and splits, we utilize an intermediate-complexity model and impose wave-1 and wave-2 stratospheric heating perturbations spun-off from a control run. At longer lags, the tropospheric response is found to be insensitive to both the wavenumber and location of the imposed heating, in agreement with freely evolving displacements and splits identified in the control run. At shorter lags, however, large differences are found between displacements and splits in both the control run and the different wavenumber-forced events. In particular, in the control run, the free-running splits have an immediate barotropic response throughout the stratosphere and troposphere whereas displacements take 1–2 weeks before a near-surface response becomes evident. Interestingly, this barotropic response found during CTRL splits is not captured by the barotropically forced wave-2 events, indicating that the zonal-mean tropospheric circulation is somehow coupled with the generation of the wave-2 splits. It is also found that in the control run, displacements yield stronger Polar-Cap temperature anomalies than splits, yet both still yield similar magnitude tropospheric responses. Hence, the strength of the stratospheric warming is not the only governing factor in the surface response. Overall, SSW classification based on vortex morphology may be useful for subseasonal but not seasonal tropospheric prediction.

Plain Language Summary The polar vortex - a strong jet that circumnavigates the stratospheric winter Pole at ~10–50 km – is known to influence surface weather. In particular, when the polar vortex becomes highly disturbed in events known as sudden stratospheric warmings, a downward influence on the surface is observed. Recent studies have debated whether the two types of sudden stratospheric warming - displacement events when the vortex is displaced off the Pole and split events when the vortex splits into two smaller vortices - have differing near-surface impacts. Here, using an idealized model, we examine the near-surface response to imposed stratospheric (longitudinally asymmetric) displacement- and split-like events. We find that on seasonal timescales (i.e., approximately longer than 3–4 weeks), the surface response is insensitive to displacements and splits. However, on subseasonal timescales (less than a month), clear differences are apparent, with splits initially leading to a stronger surface response and displacements taking 1–2 weeks for a response to develop. Further, varying the location of both the displacement- and split-type forcing does not yield appreciably different tropospheric responses. Overall, our study suggests that knowledge of the sudden stratospheric warming type is useful for subseasonal weather prediction but may not be useful in improving weather prediction on seasonal timescales.

1. Introduction

Extreme variability of the stratospheric polar vortex is understood to influence near-surface weather via downward coupling with the tropospheric eddy driven jet (e.g., Baldwin & Dunkerton, 2001; Sigmond et al., 2013). Sudden stratospheric warmings (SSWs) are examples of such extreme variability that can lead to a negative phase of the North Atlantic Oscillation (NAO) or annular mode and can persist for up to 2 months, having implications for subseasonal to seasonal weather forecasting. However, not all SSWs lead to a downward impact (e.g., Karpechko et al., 2017; Runde et al., 2016).

It has been suggested that the type of SSW, be it a displacement or split event, is important for the tropospheric response (Hall et al., 2021; Mitchell et al., 2013; O'Callaghan et al., 2014; Seviour et al., 2013). In particular, Mitchell et al. (2013) found using ERA-40 reanalysis, that split SSWs lead to an overall stronger near-surface response for two months after the onset date as compared to displacements. However, this result is not robust to SSW definition, as Charlton and Polvani (2007) found there to be no difference between the two using an alternative identification algorithm (also found by Jucker, 2016). Conversely, using a chemistry-climate model with an order of magnitude larger number of events, White et al. (2019) found instead that displacements have a slightly stronger and longer lasting tropospheric response than splits. Nevertheless, Maycock and Hitchcock (2015) found that differences between splits and displacements were small relative to natural variability, so that a very large sample size is required to conclusively identify any salient features. Most recently, Hall et al. (2021) found using ERA-Interim reanalysis that differences between displacements and splits are apparent in surface temperature, but only at lags close to the date of surface impact. However, they found insignificant differences in the NAO strength and duration at longer lags. In previous studies therefore, there is no consensus as to whether SSW type plays a role in the downward impact, and if so, at which lags during the SSW evolution, any differences are salient.

In examining the tropospheric response to SSWs, a number of studies have imposed zonally symmetric heating perturbations to the stratosphere (e.g., Kushner & Polvani, 2004; Polvani & Kushner, 2002). However, these studies imposed thermal perturbations continuously in order to examine the climatological or seasonally evolving tropospheric response. Most recently, White et al. (2020) imposed high-latitude thermal perturbations for just a few days so as to capture the 'sudden' nature of an SSW. Despite the lack of planetary-wave momentum torques which drive real SSWs, they found that the tropospheric response at longer lags was essentially indistinguishable between free-running and forced SSWs. They concluded that the tropospheric response is generic to a zonally symmetric heating in the stratosphere.

We build upon the work of White et al. (2020) and use the same idealized moist model (Jucker & Gerber, 2017) to apply zonally asymmetric (wave-1 or wave-2) heating perturbations to the stratosphere for only a few days centered at different longitudes. This allows us to examine whether the longer-term tropospheric response is dependent on the SSW type (be it a displacement or a split) and on the vortex location. The longer-term response is defined here as around 3–4 weeks after the SSW onset and is chosen to approximately match the timescale by which the splits and displacements in our control run become indistinguishable in the stratosphere.

Previous studies have imposed zonally asymmetric stratospheric anomalies to examine how polar-vortex anomalies can influence the tropospheric circulation. In particular, Smy and Scott (2009) examined the stratospheric influence on tropospheric baroclinic instability and Charlton et al. (2005) examined whether the tropospheric response to a displacement-type SSW (at 45°E) was consistent with a non-local stratospheric influence via hydrostatic and geostrophic adjustment (Ambaum & Hoskins, 2002). However, to our knowledge, there have been no studies that have tested the tropospheric response to the phasing of split and displacement SSWs.

Further motivation is provided by Zhang et al. (2016). Using reanalysis data and model simulations, they found that the polar vortex has shifted toward Eurasia in recent decades in response to Arctic sea-ice loss and suggest that such a shift has had a subsequent influence on surface weather with cooling over Europe and North America. Our experiments aim to shed some light on whether such a shift in the vortex can indeed yield near-surface differences on seasonal timescales.

We introduce the model setup and our idealized experiments in Section 2. In Sections 3 and 4 we present the results and in Section 5, a short summary.

2. Model Setup

We use the model of an idealized moist atmosphere (MiMA) developed by Jucker and Gerber (2017). MiMA includes a more comprehensive treatment of radiation than a dry dynamical core that has been used extensively in the past (e.g., Domeisen et al., 2013; Polvani & Kushner, 2002) and hence, is more suited to studying the interaction between dynamics and thermodynamics. In terms of the model setup, we follow Garfinkel,

et al. (2020b), to which we refer the reader, but with some minor changes to the Pacific Ocean heat fluxes (see Supplementary Text S4 and Tables S1-S2). Note that the model used here is slightly different to that used in White et al. (2020) which followed the setup of Garfinkel, et al. (2020a). Nevertheless, perturbation experiments (see Section 2.2) using the same setup as White et al. (2020) yield similar results.

2.1. Control Run

First, we run a control run (CTRL) for 49 years (360-day years) after discarding an initial spin-up of 10 years to allow the mixed-layer ocean to equilibriate. The integrations are all run at T42 horizontal resolution (2.8° x 2.8°) with 40 vertical levels up to ~0.01 hPa. We note that the CTRL climatology and in particular, the stationary waves are quite realistic following Garfinkel, et al. (2020a) and Garfinkel, et al. (2020b), and are comparable to that of Coupled Model Intercomparison Project Phase 5 (CMIP5) models.

We identify displacement- and split-type SSWs in CTRL to facilitate comparison with the wave-1 and wave-2 thermally forced SSWs described in Section 2.2. To identify such SSW types, we use the two dimensional moment analysis of the geopotential height Z at 10 hPa, described by Seviour et al. (2013). The December-March climatological-mean Z is used to define the vortex edge and displacements and splits are identified as the most equatorward 5% of daily centroid latitudes, and largest 5% of daily aspect ratios yielding thresholds of 70.45°N and 2.25, respectively. These ratios are slightly different than those used in Seviour et al. (2013) who used the most equatorward 5.7% of daily centroid latitudes, and largest 5.2% of daily aspect ratios in ERA-Interim reanalysis in order to approximately match the observed frequencies of splits and displacements in prior studies. The choice of thresholds using this method is somewhat subjective and we have tested our conclusions using different values. In particular, we have also utilized centroid latitude and aspect ratio thresholds corresponding to the 2.5% percentiles, yielding 33 displacements and 32 splits. Similar results are found using this smaller subset of events (compare Figures 2 and 3 in Section 3 with Figures S2–S3).

In order to increase the number of SSWs of each type in our analysis, we also identify SSWs in an additional four 49 years control runs that have slightly different initial conditions to CTRL. These initial conditions consist of changes in the imposed q-fluxes and albedo and namelist parameters for the gravity-wave parameterization that we do not go into the details of here. However, note that removing these extra events from the composites shown in Section 3 does not change the results therein. Overall, including all five control runs, there are 67 splits and 61 displacements in 245 years, yielding a frequency of 0.52 events per year which should be compared with an observed frequency of 0.68 events per year in Butler et al. (2015) using the moments definition of Seviour et al. (2013). This slight discrepancy in SSW frequency is consistent with the strong vortex bias present in MiMA compared to in ERA-5 reanalysis (see Figure S1). Note that in Sections 3–4, the combined 67 splits and 61 displacements from the five control runs as opposed to just the sub-sample of events from CTRL, are compared with the perturbation (PTRB) events, and are referred to as the control-run displacements and splits.

2.2. Perturbation Experiments

We extend the experiments of White et al. (2020) by imposing a zonally asymmetric thermal forcing in the stratosphere switched on every January 1st in the 49 years CTRL (note that we do not utilize the extra four control runs in these experiments). In particular, we add the following forcing term to the temperature tendency equation:

$$F(\lambda,\varphi,p,t) = \max[\underbrace{\tau_S(t)\Phi_S(\varphi)}_{\text{Symmetric}},\underbrace{\tau_A(t)\Phi_A(\lambda,\varphi)}_{\text{Asymmetric}}]\Lambda(p) \quad (1)$$

where

$$\tau_S(t) = \begin{cases} 1, & \text{if } 0 < t - t_0 \leq N_S \text{ days} \\ 0, & \text{otherwise,} \end{cases} \quad (2)$$

$$\tau_A(t) = \begin{cases} 1, & \text{if } 0 < t - t_0 \le N_A \text{ days} \\ 0, & \text{otherwise,} \end{cases} \tag{3}$$

$$\Phi_S(\varphi) = \frac{Q_S}{2}\left(1 - \tanh\left[\frac{\varphi - \varphi_S}{\Delta\varphi}\right]\right), \tag{4}$$

$$\Phi_A(\lambda,\varphi) = Q_A \max\left[0, \cos\left(\frac{k\pi}{180}[\lambda - \lambda_0]\right)\right]\sin\left(\pi\frac{\varphi - \varphi_L}{\varphi_H - \varphi_L}\right) \tag{5}$$

and

$$\Lambda(p) = \begin{cases} \dfrac{p - p_b}{p_t - p_b}, & \text{if } p_t < p < p_b \\ 1, & \text{if } p \le p_t \\ 0, & p > p_b. \end{cases} \tag{6}$$

In these equations, t, φ, λ, p, are the model time, latitude, longitude, and pressure, Q_S and Q_A are the zonally symmetric and zonally asymmetric heating rates (units of K day^{-1} although hereafter we drop the units for brevity), N_S and N_A are the prescribed duration (in days) of Q_S and Q_A, respectively, k is the zonal wavenumber of the heating and λ_0 is the center of the first ridge east of the prime meridian. Only these parameters are varied in this study (although note that N_A is fixed constant; see Section 4.1 for reasoning). All of the other parameters in Equations 1–6 are fixed in our study and are defined in Table 1. Note that runs with purely zonally symmetric forcing (Equation 4 and with $Q_A = 0$) are as in White et al. (2020).

Figure 1 shows example wave-1 ($k = 1$, $\lambda_0 = 225$E that is in phase with the climatological 10 hPa stationary wave 1) and wave-2 ($k = 2$, $\lambda_0 = 90$E that is out of phase with the climatological 10 hPa stationary wave 2) forcings, respectively, with $Q_S = 3$ and $Q_A = 6$. These heating rates are chosen so as to approximately match the composited Polar-Cap area-averaged, vertically integrated $\overline{T}$ anomalies in the CTRL displacements (see later Figure 4 and associated discussion). A list of experiments used in this study is given in Table 2. Note that in all of our experiments, the lower boundary of the imposed heating is defined as $p_b = 150$ hPa so as to limit the heating to the stratosphere (see Table 1).

Observed split and displacement SSWs are associated with a zonally symmetric warming that encompasses the Polar Cap along with regional maxima (e.g., Figure 1 of Butler et al., 2017). To approximate this, we include a zonally symmetric heating (Equation 4) in addition to the zonally asymmetric part of the warming with the latter chosen to be double that of the former (e.g., see Figure 1). We also remove the temperature trough of the Q_A forcing (indicated by the max [0, cos (...)] function in Equation 5).

In these PTRB runs, the focus is on the longer-lag tropospheric response to the imposed forcing. These integrations are not well suited to investigating the differences at early lags between the control-run displacements and splits, i.e., the initial downward propagation to the troposphere. This is in part due to the complicating factor of the Eliassen adjustment (Eliassen, 1951) to imposed thermal forcing at lags close to the forcing. This adjustment manifests as a meridional circulation that in the case of thermal forcing, leads to a meridional circulation in the opposite sense to that found during the onset of free-running SSWs as in the control run (e.g., see Figure 10 in White et al., 2020). This adjustment can therefore interfere with the downward propagation and one must be careful at teasing apart the process by which anomalies actually propagate downward to the troposphere from the Eliassen adjustment. Following White et al. (2020), we therefore focus primarily on the long-term response (~3–4 weeks onwards) in the PTRB runs. Nevertheless, as will be seen in the next section, this longer-term response timescale pops out as a somewhat natural timescale in the control SSWs.

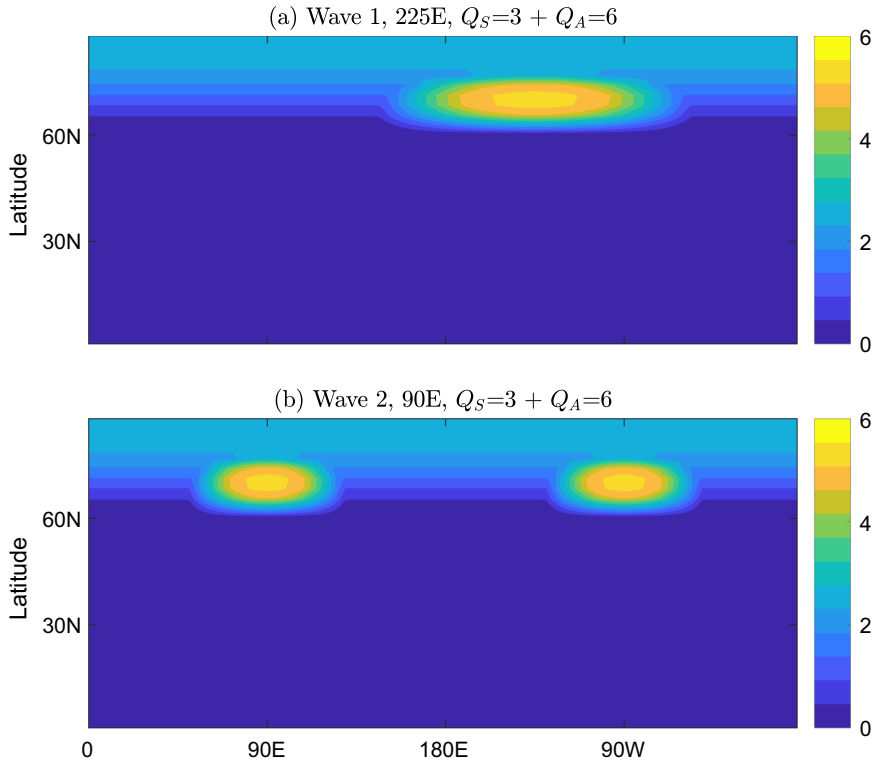

Figure 1. Example mixed zonally symmetric (Q_S = 3K day^{-1}) and zonally asymmetric (Q_A = 6K day^{-1}) thermal forcing at 10 hPa for (a) wave-1 with λ_0 = 225E that is in phase with the climatological 10 hPa stationary wave 1, and (b) wave 2 with λ_0 = 90E that is out of phase with the climatological 10 hPa stationary wave 2.

3. Control Run Displacements and Splits

We begin by compositing the 67 split and 61 displacement control-run SSWs (i.e., from all five control runs) in Figure 2. To calculate the Northern Annular Mode (NAM) index we use the geopotential-height (Z) method of Baldwin and Thompson (2009) wherein Z anomalies are first calculated as deviations away from the daily climatology, then area averaged over 60–87 N, before being divided by the standard deviation and multiplied by −1. Close to the onset date, the NAM has a much more barotropic structure during the splits than the displacements, extending down close to the surface (Figures 2a and 2b). In the stratosphere, this barotropic structure agrees with Esler and Scott (2005), whereas the extension into the troposphere agrees with splits identified in a comprehensive model by Maycock and Hitchcock (2015). Displacement events on the other hand take around one week before a lower-tropospheric negative NAM signal is apparent. Further, displacements have a more negative stratospheric NAM extending up to lag day 35. In the troposphere at longer lags, the two do not exhibit any significant differences.

The longer-term near-surface response in terms of 970 hPa u anomalies is shown in Figures 3c and 3d averaged over lags 31–90. Lag 31 is chosen to focus on the longer-lag response and this represents the approximate lag by which the initially barotropic-NAM response to split SSWs has subsided (Figure 2b). Nevertheless, the results are fairly insensitive to varying these lags, e.g., averaging from lag 21 onwards. As with the NAM, the near-surface response to the control-run splits and displacements are similar, with a clear equatorward shift of the jet in the North Atlantic and more of an extension of the jet downstream in the Central/Eastern Pacific. This extension into the Eastern Pacific, is more enhanced for the displacements. Overall, the surface response is more zonally symmetric in MiMA than in composites of observed SSWs (e.g., Figure 1 in Hitchcock & Simpson, 2014) which show a clear preferred basin structure. However, the surface response still projects onto the NAM (first empirical orthogonal function; Figure S4).

As aforementioned, the response to the control-run displacements and splits become statistically indistinguishable after approximately 3–4 weeks in the lower stratosphere (and even earlier in the troposphere

Table 1
Table of parameters used in the PTRB experiments (see Equations 1–6) along with their units and a description

Parameters varied in this study		
Parameter symbol	Units	Description
K		Zonal wavenumber of heating
λ_0	°	Longitude of first ridge east of Prime Meridian
Q_S	K day^{-1}	Zonally symmetric heating rate
Q_A	K day^{-1}	zonally asymmetric heating rate
N_S	Days	Time duration of symmetric heating (either = 0 or = 10 here)
Parameters fixed in this study		
Parameter symbol	Units	Description
t_0	S	First timestep at which the heating is turned on (12a.m. on January 1st)
$N_A = 10$	Days	Time duration of asymmetric heating
$p_t = 60$	hPa	Top level of linear reduction in heating
$p_b = 150$	hPa	Bottom level of linear reduction in heating
$\varphi_S = 60$	°	Latitude at which symmetric heating reaches half of Q_S
$\Delta\varphi = 5$	°	Latitudinal half-width of symmetric heating
$\varphi_H = 80$	°	Upper latitudinal limit of asymmetric heating
$\varphi_L = 60$	°	Lower latitudinal limit of asymmetric heating

Note: Top part of table shows the parameters that are varied in our PTRB experiments, whereas bottom part lists the fixed-value parameters. PTRB, perturbation.

Table 2
List of PTRB experiments used in this study

Wave-1 experiments ($k = 1$)		
Forcing magnitude (K day^{-1}) and duration	Longitude of 1st ridge (λ_0)	Text description
$Q_S = 0$, $Q_A = 12$ ($N_A = 10$)	45E (out of phase)	Asymmetric
	225E (in phase)	
	315E (in quadrature)	
$Q_S = 3$, $Q_A = 6$ ($N_S = N_A = 10$)	45E (out of phase)	Symmetric and Asymmetric
	225E (in phase)	
	315E (in quadrature)	
Wave-2 experiments ($k = 2$)		
Forcing magnitude (K day^{-1}) and duration	Longitude of 1st ridge (λ_0)	Text description
$Q_S = 0$, $Q_A = 12$ ($N_A = 10$)	0E (in phase)	Asymmetric
	45E (in quadrature)	
	90E (out of phase)	
$Q_S = 3$, $Q_A = 6$ ($N_S = N_A = 10$)	0E (in phase)	Symmetric and Asymmetric
	45E (in quadrature)	
	90E (out of phase)	
$Q_S = 0$, $Q_A = 8$ ($N_A = 10$)	0E (in phase)	Asymmetric
	90E (out of phase)	
$Q_S = 2$, $Q_A = 4$ ($N_S = N_A = 10$)	0E (in phase)	Symmetric and asymmetric
	90E (out of phase)	

Note: In-phase, out-of-phase and in quadrature refer to the phasing of the forcing with the 10 hPa climatological stationary waves.

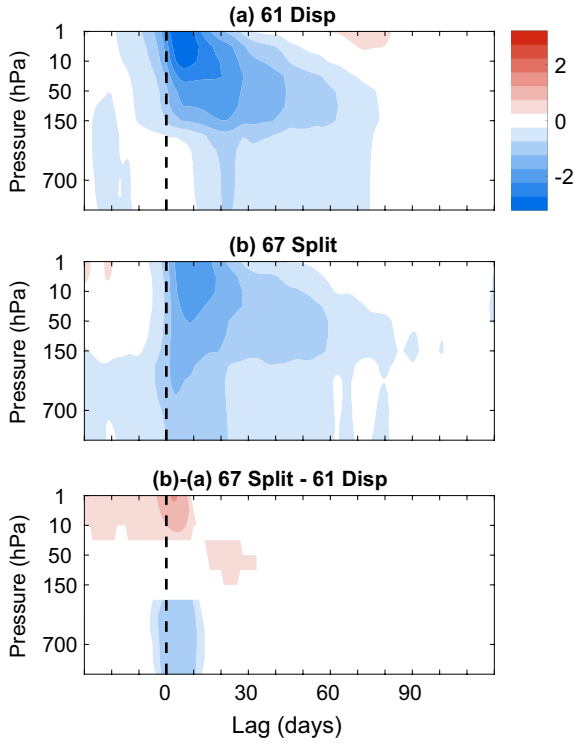

Figure 2. Northern Annular Mode (NAM) composites of the control-run displacements (61 events; top), splits (67 events; middle) and splits-displacements (bottom). Units are in standard deviations. In (b)–(a), only significant differences at the 95% level using a standard student's t-test are plotted.

and middle-to-upper stratosphere; Figure 2). At earlier lags however, the differences are large and represent the initial downward transmission to the troposphere. It is for this reason that the remainder of the manuscript focusses on the longer-lag response to such events. For the PTRB runs discussed in the next section, this longer-lag focus also ensures that issues associated with the Eliassen adjustment to the imposed heating (see Section 2.2) are circumvented.

4. Idealized Experiments

In order to isolate the importance of zonal asymmetries in the warming for the longer-term surface impact, we impose in the stratosphere either: (1) A zonally asymmetric warming augmented with a weaker zonally symmetric warming, or (2) a zonally asymmetric warming, and in both cases, vary the phase of the asymmetric part of the warming. This allows us to understand whether the location of the vortex anomalies is important for the surface response.

Note that herein, anomalies are calculated as deviations away from the daily climatology in the 49 years CTRL from which the PTRB runs are branched (see Section 2.2).

4.1. Choice of Forcing Magnitude, Duration and Location

The aim in these PTRB experiments is to impose a warming of similar magnitude to that found during the control-run SSWs. To apply a forcing of roughly the correct magnitude, we calculate area-averaged Polar-Cap (50°N − 90°N) and vertically integrated (mass-weighted over 150–1 hPa) $\overline{T}$ anomalies for the control-run displacements and splits in Figure 4. The control-run displacements and wave-1 PTRB experiments are shown on the left and the splits and wave-2 PTRB experiments on the right (control-run SSWs in solid black lines). For the PTRB wave-1 experiments it is found that setting $Q_S = 3$ and $Q_A = 6$ yields similar magnitude temperature anomalies to the control-run displacements (dashed lines in red and blue in Figure 4a). The asymmetric component is doubled compared to that of the symmetric component to ensure that the symmetric part does not overwhelm the asymmetric part of the warming which is our focus. Equivalent asymmetric forcing ($Q_A = 12$; solid lines in red and blue) also yields similar magnitude $\overline{T}$ anomalies to the control-run displacements. The magnitude of the vertically integrated $\overline{T}$ anomalies in Figure 4 may seem quite small, however, this is a result of the mass-weighting that gives greater weight to the lower stratosphere where the $\overline{T}$ anomalies are generally smaller than in the middle-upper stratosphere (not shown). It should also be noted that there is little in the way of significant differences between the various pairs of PTRB experiments (pairs tested using a student's t-test are indicated by asterisks in legend), aside from small significant differences during the recovery stage at lags 70 + . This indicates that the magnitude of the Polar-Cap warming is quite generic and is not dependent on the location of the ridge(s) during the SSW evolution.

It is clear that the control-run displacements lead to a warmer Polar Cap than the control-run splits. This is a robust feature that is also present for displacements and splits in ERA-5 reanalysis (dashed black lines) where the events are identified using the same thresholds as in Seviour et al. (2013) (i.e., a centroid latitude of 66°N for the displacements, and aspect ratio of 2.4 for the splits). Note that the differences between displacements and splits in both MiMA and ERA-5 reanalysis are significant at the 95% level up until approximately lag 15 (not shown). In terms of forcing therefore, a more appropriate heating rate is $Q_S = 2$, $Q_A = 4$ for the mixed wave-2 PTRB and $Q_S = 0$, $Q_A = 8$ for the asymmetric wave-2 PTRB (Figure 4b). We will therefore present results using both the stronger wave-2 heating (i.e., $Q_S = 3$, $Q_A = 6$) and weaker wave-2 heating (i.e., $Q_S = 2$, $Q_A = 4$).

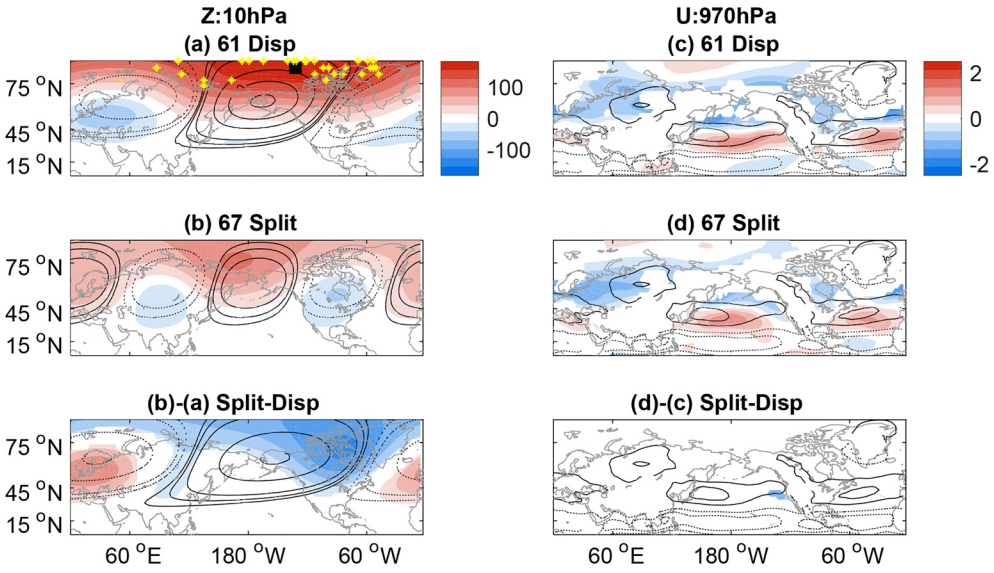

Figure 3. Regional composites of the control-run displacements (top), splits (middle) and splits-displacements (bottom) for Z anomalies at 10 hPa averaged over lags 1–3 in the left column, and u anomalies at 970 hPa averaged over lags 31–90 in the right column. Units are (left) m, and (right) ms^{-1}. Black contours in the left column indicate the climatological Z with contours at ±50, 100, 200, 300, ...m for wave-1 (top), wave-2 (middle), and the combined wave-1 and wave-2 (bottom). Black contours in right column indicate the climatological u with contours at ±4, 8, ...ms^{-1} (right). Yellow asterisks in (a) show the location of the maximum Z anomalies for each of the 61 displacements and large black square shows the average location. Significant differences in bottom row as in Figure 2.

In these PTRB experiments, the warming is chosen to be switched on for $N_S = N_A = 10$ days, which is motivated by examining the vortex morphology. In particular, Figure 5 shows that it takes ~10 days for the aspect ratio for the control-run splits to fall below the SSW threshold of 2.25 (Figure 5b) and for the centroid latitude for the control-run displacements to become northward of the SSW threshold of 70.45°N (Figure 5a). Hence, this ~10 days timescale represents the approximate length of time after the SSW onset date by which the vortex no longer satisfies the relevant SSW threshold. Nevertheless, switching on the forcing for a shorter period, say $N_S = N_A = 3$ days as in White et al. (2020) but still maintaining the same overall forcing magnitude (i.e., with $Q_S = 10$, $Q_A = 20$), yields qualitatively similar results to those presented here (not shown).

We now highlight the various locations of the zonally asymmetric forcing in our experiments. Figure 6 shows Z anomalies at 10 hPa averaged over lags 1–3 for the zonally asymmetric forced runs with $N_A = 10$ days and for the $\lambda_0 = 45$E and $\lambda_0 = 225$E wave-1 (6a,b) and the $\lambda_0 = 0$E and $\lambda_0 = 90$E wave-2 (6c,d) PTRB runs. For wave-1, these longitudes are chosen so as to either constructively ($\lambda_0 = 225$E) or destructively ($\lambda_0 = 45$E) interfere with the climatological stationary wave-1. In terms of the former, $\lambda_0 = 225$E agrees with the average location of the Aleutian High after the control-run displacement onset (~ 227E; Figure 3a), whereas $\lambda_0 = 45$E agrees with the most westward location of the Aleutian High maximum in all of the 61 control-run displacements (see yellow asterisks in Figure 3a). Note that the $\lambda_0 = 315$E experiment approximately agrees with the most eastward location of the Aleutian High maximum in the control-run displacements. These eastward and westward limits of the Aleutian-High maximum are also found if focusing on the 60 N latitude circle (which is the latitude of the climatological Aleutian High centre), which may make more sense given that the circumference of a latitude circle shrinks considerably toward the Pole. For wave-2, the $\lambda_0 = 0$E PTRB best agrees with the phasing of the ridges in the control-run splits (Figure 3d).

The influence of the forcing on the strength of the Polar Vortex is examined in Figure 7 which shows the NAM index at 100 hPa for the wave-1 (a) and wave-2 (b) PTRB experiments. All PTRB runs show a weakening of the vortex (i.e., a negative NAM) that is of similar magnitude between the various wave-1 and wave-2 experiments, a consequence of the equivalent forcing. However, none of the PTRB runs yield as negative a NAM as in the control-run displacements and splits. In fact, the control-run displacements and splits are approximately the same strength in the lower stratosphere. Conversely, above 100 hPa, the discrepancy in

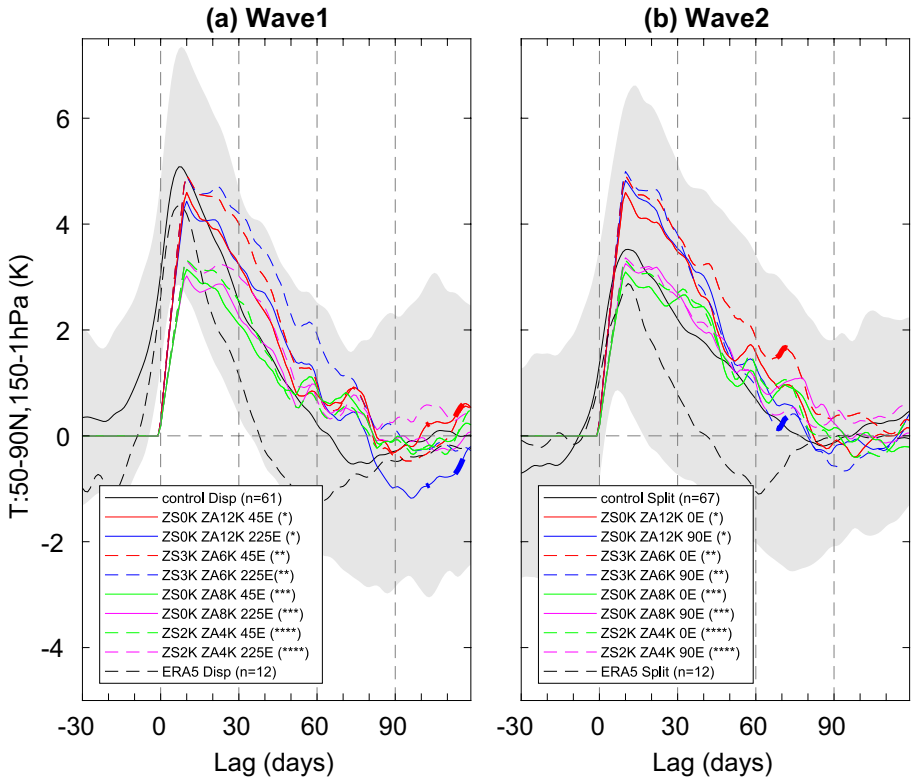

Figure 4. Timeseries of $\overline{T}$ anomalies area-averaged over 50°N–90°N and vertically integrated (mass-weighted) over 150–1 hPa for (left) control-run displacements, and various wave-1 PTRB experiments, and (right) control-run splits and various wave-2 PTRB experiments. Thick portions of the colored lines represent statistically significant differences at the 95% level between the individual pairs of experiments using a standard student's t-test (pairs are indicated by equal numbers of asterisks in brackets). Gray shading shows the black lines (i.e., control-run events) ± 1 standard deviation. See legend for details of PTRB experiments shown. Also shown are the ERA-5 displacements (a) and splits (b) over 1979–2018 defined using the same thresholds as in Seviour et al. (2013); i.e., displacements are defined when the centroid latitude becomes equatorward of 66°N, and splits are defined when the aspect ratio becomes larger than 2.4. Note that the list of events in ERA-5 here matches the list of events in the overlapping period (1979–2009) in Seviour et al. (2013).

vortex strength and warming between displacements and splits as apparent in Figure 4 becomes clearer. For instance, $\overline{u}$ at 60 N and 10 hPa clearly shows a weaker vortex for the displacements than the splits which is also the case in ERA-5 reanalysis (Figure S5 in the supplementary material). Nevertheless, our focus here is on the lower stratosphere which has been shown to be more tightly linked to the tropospheric response (e.g., Maycock & Hitchcock, 2015; White et al., 2019).

4.2. Response to Varying the Phase of Mixed Symmetric and Asymmetric Forcing

We now quantitatively assess whether the downward impact on the troposphere at longer lags depends on the wavenumber or phasing of the imposed temperature perturbation. As discussed in Section 3, free-running SSWs in the control runs can be characterized as a quasi zonally symmetric warming over the Pole along with one or two localized maxima (depending on whether the SSW is a split or displacement; e.g., Figures 3a and 3b) further equatorward.

Experiments are now performed with both symmetric and asymmetric parts of the heating not equal to zero (i.e., $Q_S \neq 0$ and $Q_A \neq 0$). In particular, we set the symmetric part as $Q_S = 3$ and the asymmetric part as $Q_A = 6$, both switched on for $N_S = N_A = 10$ days which as aforementioned, yields similar magnitude $\overline{T}$ anomalies to the control-run displacements (see Figure 4).

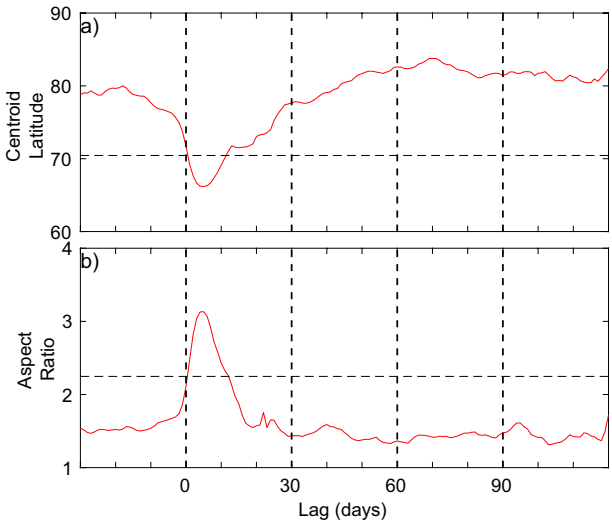

Figure 5. Timeseries of the composite centroid latitudes and aspect ratios for the control-run displacements (61 events; a) and splits (67 events; b), respectively. Dashed horizontal lines indicate the thresholds used to identify displacements (70.45°N) and splits (2.25) in this study.

The NAM index and 970 hPa u anomalies averaged over lags 31–90 are shown in Figures 8a, 8b and 9a, 9b for the $\lambda_0 = 45$E and $\lambda_0 = 225$E wave-1 runs that are out of phase and in phase with the climatological stationary wave 1, respectively (see black contours in Figures 6a and 6b). Both wave-1 runs show a classical NAM-like response with a "dripping-paint" like pattern into the troposphere as observed by Baldwin and Dunkerton (2001). In both runs, the lower-stratospheric anomalies persist for up to four months, although weaken substantially after two months. The longer NAM timescales in the lower stratosphere agree with the purely zonally symmetric thermal-forcing experiments performed by White et al. (2020) who found that this was a consequence of the relatively coarse resolution. Indeed, coarser resolution models tend to have more persistent annular mode variability (Gerber et al., 2008). Overall, there are no significant differences between the two wave-1 experiments (panel b–a) indicating that in the presence of a weaker background warming, the tropospheric response to asymmetric warming is insensitive to the vortex location. Applying the heating at $\lambda_0 = 315$E (i.e., close to the most eastward location of the Aleutian High in the control-run displacements shown in Figure 3a) also yields quantitatively similar results (not shown). In the $\lambda_0 = 0$E and $\lambda_0 = 90$E wave-2 runs (that are in phase and out of phase with the climatological stationary wave 2, respectively; see black contours in Figures 6c and 6d) shown in Figures 8c, 8d and 9c,9d, there is also little difference in the tropospheric response to the forcing location. Varying the location to $\lambda_0 = 45$E yields insignificant differences to the presented runs (not shown). Further, near-surface T (Figure S6 in the supplementary material) also shows little difference between the various wave-1 and wave-2 PTRBs with a cooling over Eurasia and warming over Eastern North America and the Mediterranean as seen in observations (e.g., Hitchcock & Simpson, 2014). Note that the wave-2 forcing applied here is barotropic in the stratosphere, yet interestingly, there is no barotropic NAM structure close to the onset date which is found in the control-run splits (Figure 2a). This provides evidence that the wave-2 growth mechanism (likely via wave resonance generating a barotropic mode; Esler & Scott, 2005) prior to the split is important for the observed barotropic signal immediately after the onset.

To determine if there are any differences between the tropospheric response at long lags to wave-1 and wave-2 forcing, i.e., to see if there are differences between displacement and split SSWs as in Section 3, composite differences are calculated between various wave-1 and wave-2 runs. The bottom-left panels in Figures 8 and 9 show the NAM and 970 hPa u differences between the mixed symmetric and asymmetric wave-1 $\lambda_0 = 45$E and wave-2 $\lambda_0 = 0$E runs with $Q_S = 3$ and $Q_A = 6$ switched on for $N_S = N_A = 10$ days (i.e., panels c–a in each figure), whereas the bottom-middle panel shows the same as the bottom left except for

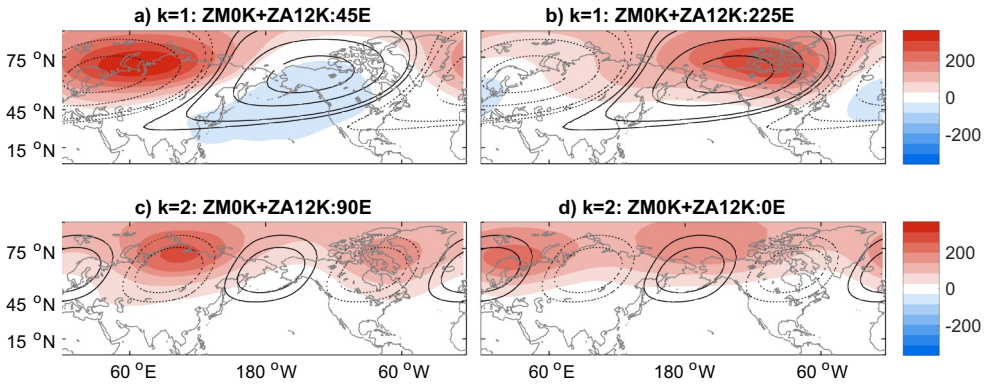

Figure 6. (Top) Z anomalies (shading) at 10 hPa averaged over lags 1–3 for the $\lambda_0 = 45$E and $\lambda_0 = 225$E wave-1 PTRB experiments (Bottom) Same as top row except for the $\lambda_0 = 90$E and $\lambda_0 = 0$E wave-2 experiments. Units in m. Black contours show the wave-1 (top) and wave-2 (bottom) climatology as in Figures 3a and 3b.

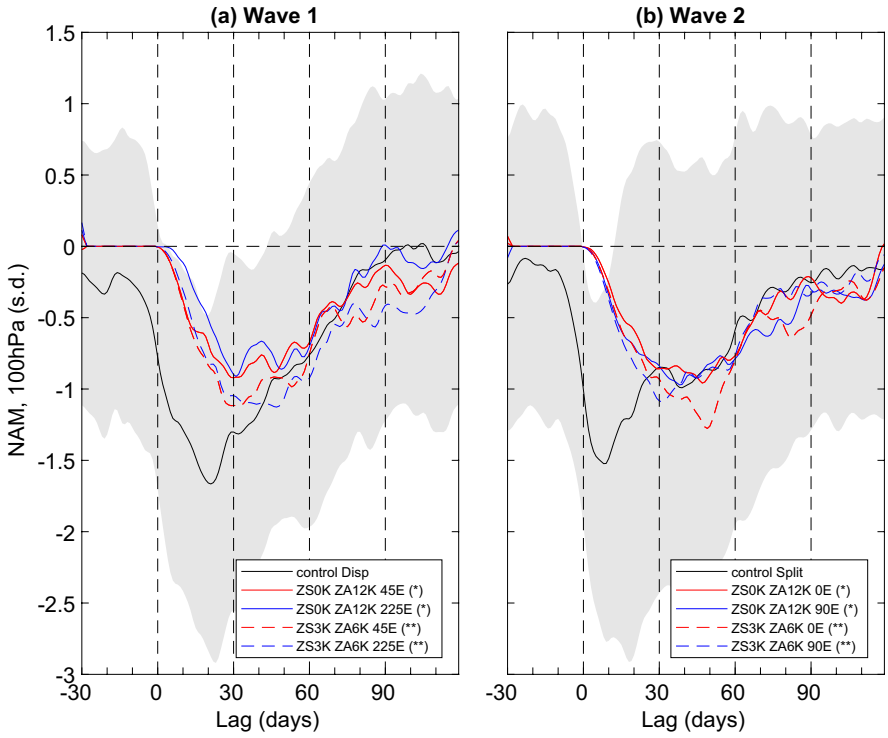

Figure 7. Timeseries of the Northern Annular Mode (NAM) index at 100 hPa for (a) control-run displacements and wave-1 PTRB experiments, and (b) control-run splits and wave-2 PTRB experiments. See legend for details of the individual PTRB experiments. Thick portions of the colored lines represent statistically significant differences at the 95% level between the individual pairs of experiments using a standard student's t-test (pairs are indicated by equal numbers of asterisks in brackets). Gray shading shows the black lines (i.e., control-run events) ± 1 standard deviation.

the mixed wave-1 $\lambda_0 = 225$E run and wave-2 $\lambda_0 = 90$E run (i.e., panels d–b). The bottom right corresponds best to the free-running displacements and splits in terms of the Z anomalies (see Figures 3a and 3b), showing the difference between the mixed $\lambda_0 = 225$E wave-1 and $\lambda_0 = 0$E wave-2 runs (panels c–b). Aside from slightly significantly more negative u anomalies over North Africa/Southern Europe in all three wave-2 runs compared to the wave-1 runs, indicating a slightly stronger jet shift in the latter, there is little else that is significantly different. This indicates that the tropospheric response is insensitive to the location of the child vortices in the stratosphere when a weaker background warming is also present.

To better compare the magnitudes of the surface response across the various PTRB experiments, Figure 10a shows zonal-mean zonal wind $\overline{u}$ 970 hPa anomalies averaged over lags 31–90 for wave-1 PTRB experiments and the control-run displacements and Figure 10b shows the same except for wave-2 PTRB and the control-run splits (in both panels see red and blue dashed lines for PTRB and solid black lines for control events). It is clear that the mixed symmetric and asymmetric PTRBs (red and blue dashed lines) project onto the tropospheric NAM with a dipole straddling the climatological jet maximum. Nevertheless, the anomalies are stronger than in the control-run displacements and splits (particularly on the poleward flank of the jet), indicating that even though the integrated stratospheric temperature anomalies are approximately equal between the PTRB and the control-run events (Figure 4), there is some other additional factor that governs the strength of the tropospheric response. The two mixed PTRB experiments yield similar magnitude, statistically-insignificant responses in $\overline{u}$ for both wave-1 and wave-2 indicating that in a more realistic forcing setup with a background warming in addition to the stronger asymmetric warming, the tropospheric response is insensitive to the vortex phasing.

We also here document differences in 970 hPa $\overline{u}$ anomalies between the various mixed runs at lags 21–30 in Figure 11. Figure S9 in the supplementary material shows regional 970 hPa u anomalies at these lags (akin to that shown for lags 31–90 in Figure 9 here). In the control runs, both the displacements and splits (black lines) project onto the tropospheric NAM with a similar dipole as found at lags 31–90

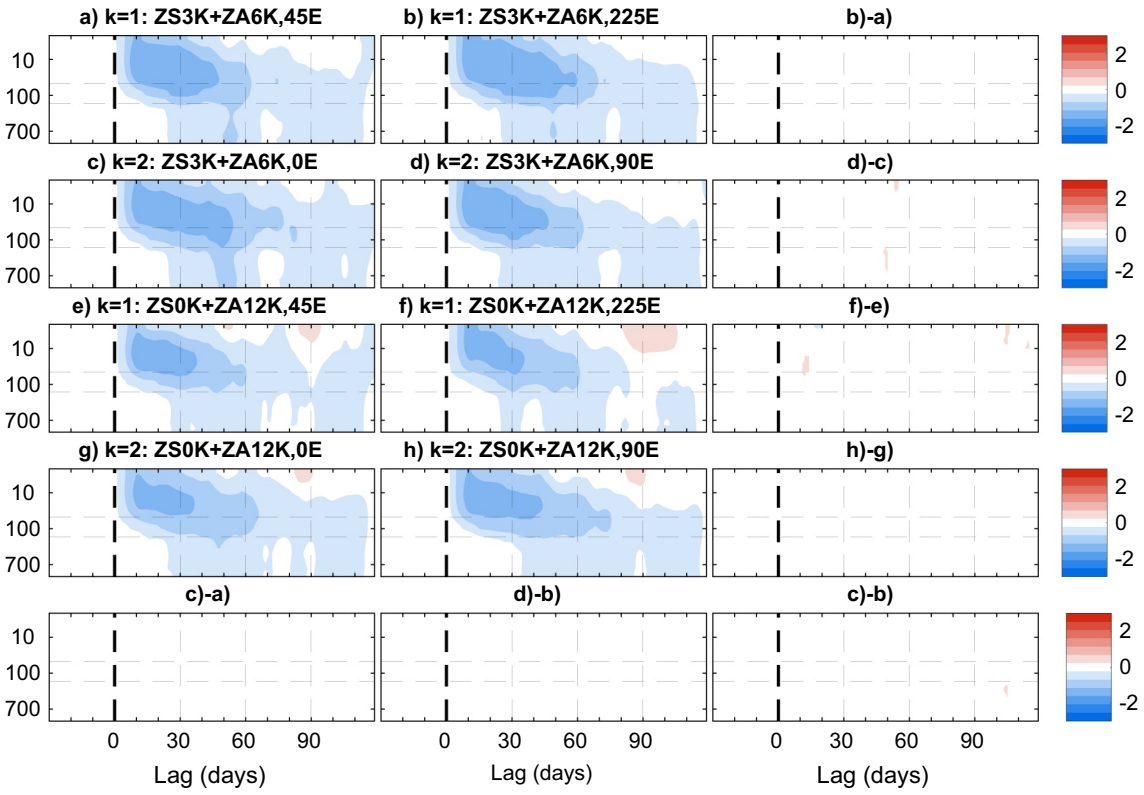

Figure 8. (Top row): NAM index composites for the mixed symmetric and asymmetric (i.e., $Q_S = 3$, $Q_A = 6$) $\lambda_0 = 45$E and $\lambda_0 = 225$E wave-1 PTRB runs with $N_S = N_A = 10$ days. (Second row): Same as top row except for the $\lambda_0 = 0$E and $\lambda_0 = 90$E wave-2 PTRB runs. (Third and fourth rows): Same as top two rows except for the asymmetric (i.e., $Q_S = 0$, $Q_A = 12$) PTRBs with $N_A = 10$ days. Right column for the top four rows show the composite difference between the middle and left columns. (Bottom row): Composite differences (c)-(a), (d)-(b), and (c)-(b). Difference panels only show points that are significantly different at the 95% level using a standard student's t-test.

(Figures 9–10) but with the displacements leading to a slightly stronger jet shift than splits. At earlier lags (not shown), the splits have a larger jet shift in agreement with the NAM index in Figure 2. For both the wave-1 and wave-2 PTRBs however, there is not a clear projection onto the tropospheric NAM. For instance, for wave-1, the $\lambda_0 = 225$E runs lead to more of a double-peak structure with $\overline{u} > 0$ anomalies at 40 N and 60 N whereas the $\lambda_0 = 45$E runs lead to a dipole that is too far poleward compared to that expected for a projection onto the tropospheric NAM (with a significant difference between the two runs). Regionally, the mixed wave-1 $\lambda_0 = 225$E run does not project onto the tropospheric NAM over the North Atlantic unlike in the $\lambda_0 = 45$E run (Figure S9). There are similar differences for the wave-2 PTRBs, with an overall lack of a consistent projection onto the canonical NAM pattern. The two wave-2 mixed runs (i.e., both $\lambda_0 = 0$E and $\lambda_0 = 90$E) for example, exhibit dipoles that are located too far poleward, with the maximum $\overline{u}$ anomaly occurring near the climatological jet maximum, and the minimum occurring northward of 75°N. However, note that differences between the various pairs of experiments are generally insignificant.

It may be surprising that at lags 21–30, the tropospheric response varies so much between various PTRB runs, especially considering the similarity between lags 11–20 and lags 21–90 in $\overline{u}$ anomalies found in the zonally symmetric forced runs of White et al. (2020) (their Figure 2). This is likely due to two reasons: (1) the forcing in White et al. (2020) had no zonal heterogeneities unlike here (although note that the forcing here still projects onto wave-0), and (2) the thermal forcing was switched on for $N_S = 3$ days in White et al. (2020), whereas here it is switched on for $N_S = N_A = 10$ days. The Eliassen adjustment during the forcing stage (see Section 2.2 for more details) and the subsequent rearrangement of the stratospheric and tropospheric circulation takes longer when the forcing has a longer duration. Due to this, it is difficult to

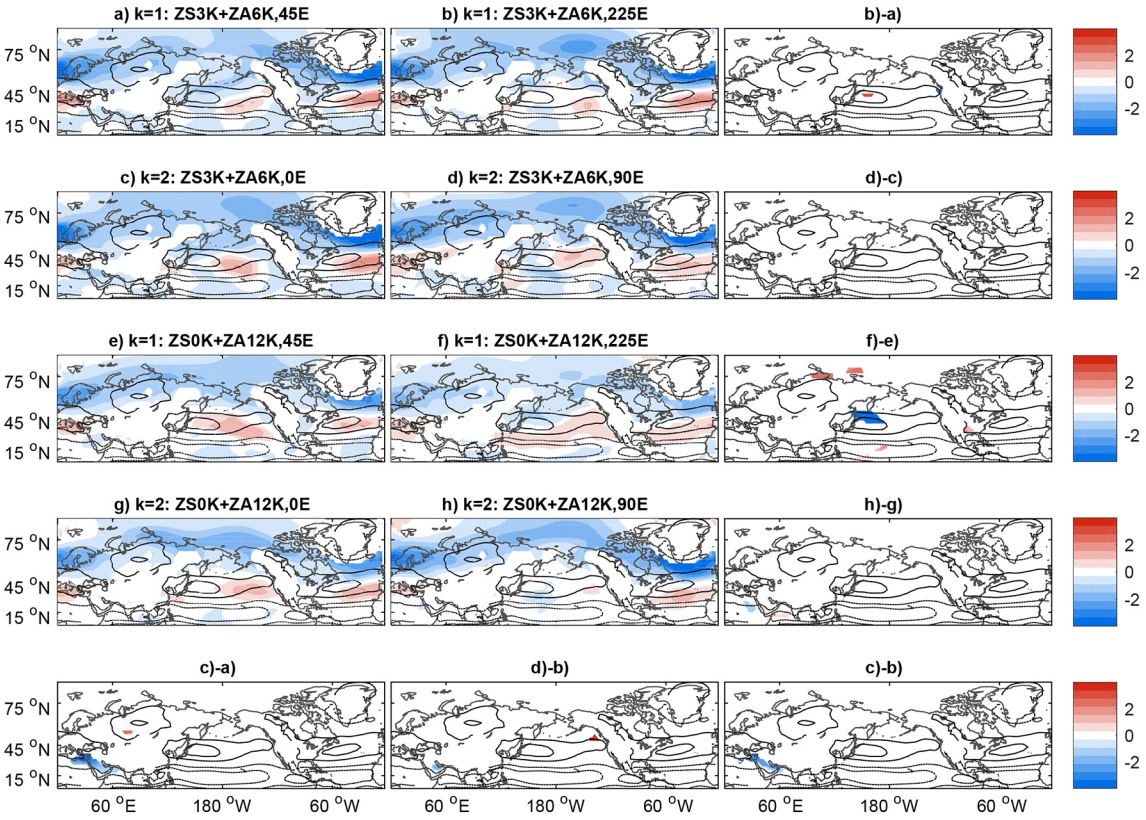

Figure 9. Same as Figure 8 except for u anomalies at 970 hPa averaged over lags 31–90. Black contours as in Figure 3c. Note that the difference panels are doubled in magnitude to aid visibility.

determine if these anomalies at lags close to the forcing in the PTRB experiments are meaningful in terms of the downward transmission of the NAM anomalies.

4.3. Response to Varying the Phase of Asymmetric Forcing

In the previous section, the mixed zonally symmetric and zonally asymmetric forcing runs produced a similar tropospheric NAM response to the control-run SSWs. The forcing in these mixed experiments are designed to mimic free-running SSWs that have warm anomalies encompassing the Polar Cap north of ~70°N–75°N, with an asymmetric component further equatorward (e.g., Figures 3a and 3b). However, the relative importance of the symmetric, more poleward part of the warming, and the asymmetric, more equatorward part of the warming, for the near-surface NAM response is not known. Many studies have found that zonally symmetric stratospheric forcing encompassing the Polar Cap projects onto the tropospheric NAM (e.g., Butler et al., 2010; Song & Robinson, 2004; White et al., 2020), but it is less known if asymmetric forcing (i.e., the eddy component) also yields a tropospheric NAM-like response. It should be noted however, that in the asymmetric runs presented in this section, because we remove the troughs of the heating in Equation 5, the asymmetric heating still projects onto wave-0 (i.e., onto the zonal-mean) and thus yields a net warming. This can be seen most clearly in Figure 4 whereby both the mixed symmetric-asymmetric runs, and the asymmetric runs, yield approximately equivalent Polar-Cap $\overline{T}$ anomalies (e.g., compare the dashed and solid red and blue lines in Figure 4).

We thus now impose zonally asymmetric heating (with $Q_S = 0$) to isolate the importance of the wave-1 or wave-2 eddy part of the SSW in the tropospheric response. The magnitude of the presented asymmetric experiments is chosen to be $Q_A = 12$ which is equivalent in magnitude to the mixed $Q_S = 3$, $Q_A = 6$ runs presented in the previous section (as aforementioned, both yield similar magnitude Polar-Cap $\overline{T}$ anomalies

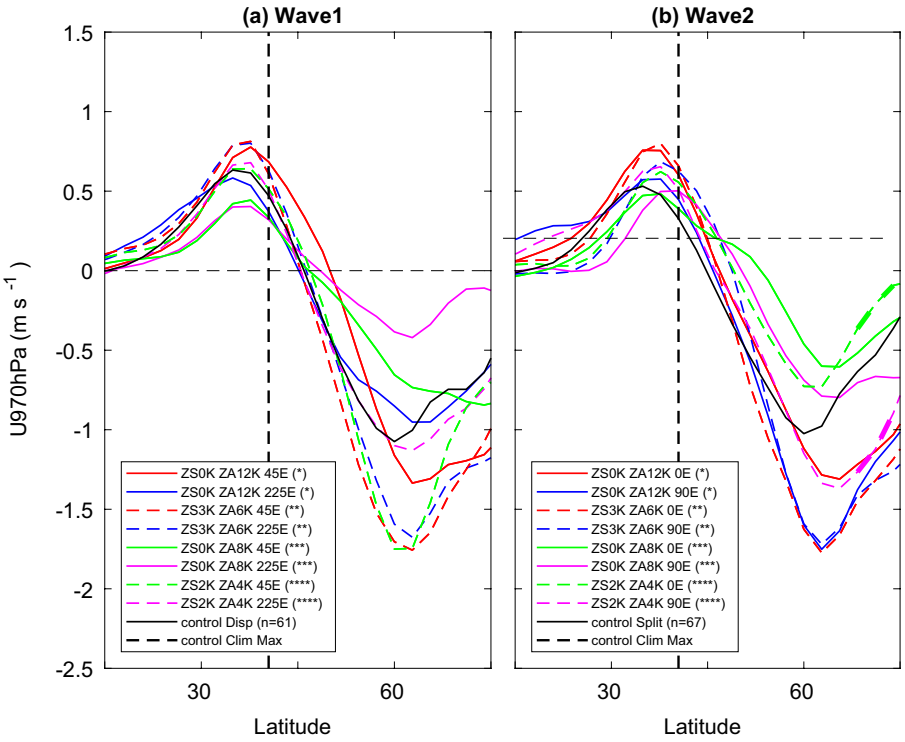

Figure 10. Latitudinal profiles of zonal-mean zonal wind $\overline{u}$ anomaly composites at 970 hPa averaged over lags 31–90 for (a) various wave-1 PTRB experiments and control-run displacements, and (b) for wave-2 PTRB experiments and control-run splits (see legend for details). PTRB experiments are shown in colored lines and control-run SSWs are shown in black lines. Thick vertical black line indicates the December-February climatological $\overline{u}$ maximum. Thick portions of the colored lines represent statistically significant differences at the 95% level between the individual pairs of experiments using a standard student's t-test (pairs are indicated by equal numbers of asterisks in brackets).

as shown in Figure 4). A forcing duration of $N_A = 10$ days is again chosen to approximate the timescale by which the control-run displacements and splits no longer satisfy the relevant SSW criteria (Figure 5).

Figures 8e and 8f and Figures 9e and 9f show the NAM index and 970 hPa u averaged over lags 31–90 for the $\lambda_0 = 45$E (e) and $\lambda_0 = 225$E (f) wave-1 PTRB runs with the heating switched on for $N_A = 10$ days. Overall, these zonally asymmetric runs produce qualitatively similar NAM indices and u anomalies to the mixed zonally symmetric-asymmetric forcing in Section 4.2 but with weaker magnitudes, particularly in the tropospheric response (Figure 9; compare top two rows with third and fourth rows). Although generally insignificant, there are differences between the two wave-1 runs, with the $\lambda_0 = 45$E run (i.e., heating that is out of phase with climatological wave-1) yielding a slightly stronger tropospheric response that is significantly different over the Western Pacific and at higher latitudes (panel f–e; also see Figure 10a). The same is true for the $\lambda_0 = 0$E and $\lambda_0 = 90$E wave-2 PTRB runs (Figures 9g and 9h), with the heating that is out-of-phase with stationary wave-2 ($\lambda_0 = 90$E), yielding a stronger North Atlantic jet shift as well as stronger anomalies over the North Pacific (although note that they are insignificantly different; also see Figure 10b).

Despite the lack of differences between the various wave-1 and wave-2 experiments (both here and in Section 4.2), it is worthwhile noting that the near-surface response to these PTRB experiments is not identical to that of the control-run displacements and splits (Figure 3). In particular, the North-Atlantic/Canada anomalies are more robust and stronger across all runs than the anomalies in the North-Pacific basin (Figure 9). This was not the case in the control-run events that yielded similar anomalies over the two regions. The reason for this appears to be due to asymmetries in Z' anomalies at longer lags. Figures S7-S8 show Z' anomalies at 10 hPa and 100 hPa averaged over lags 31–90. There are asymmetries present at both levels, although at 100 hPa, all runs, no matter where the initial heating is located, show a peak over the North Atlantic/Canada. This qualitative pattern is also evident at levels below 100 hPa (not shown). Such anomalies

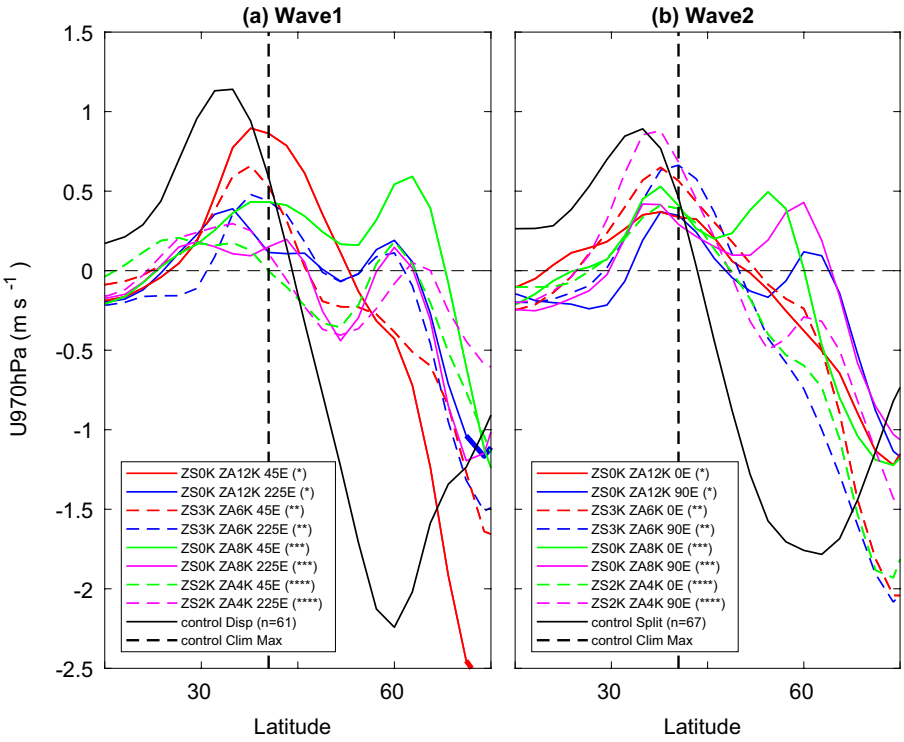

Figure 11. Same as Figure 10 except for $\overline{u}$ averaged over lags 21 to 30.

are in agreement with the arguments of Ambaum and Hoskins (2002) who suggested that the compression of the column of air below the vortex is responsible for the negative tropospheric NAM. However, one should be wary to draw conclusions as the Z' anomalies here are an order of magnitude larger than the corresponding anomalies in the CTRL events (not shown). We are currently undertaking further work using these experiments to better gauge how important the arguments of Ambaum and Hoskins (2002) are for the surface response.

Overall therefore, the asymmetric part of the warming yields a projection onto both the stratospheric and tropospheric NAM, indicating that the eddy part of the warming is sufficient to generate a longer-term tropospheric NAM response (although note that the asymmetric forcing by construction, projects onto wave-0 in the stratosphere and leads to a net warming). Thus, with the forcing magnitudes used in this section, the location of the heating does not appear to matter for the magnitude of the near-surface response.

4.4. Applying Differential Wave-1 and Wave-2 Forcing

In Figure 4 it was noted that the control-run splits are associated with weaker stratospheric Polar-Cap temperature anomalies than the control-run displacements despite the two having near-indistinguishable tropospheric responses at long lags. In Sections 4.2-4.3, equal magnitude forcing was applied that yielded $\overline{T}$ anomalies that were approximately equivalent to those in the control-run displacements. In this section, we now compare the tropospheric response to differential heating with the same wave-1 heating as in Sections 4.2–4.3, but with weaker wave-2 heating that approximately yields the same integrated $\overline{T}$ anomalies as in the control-run splits (see pink and green lines in Figure 4b).

Figure 12 shows 970 hPa u anomalies averaged over lags 31–90 for the $\lambda_0 = 45$E and $\lambda_0 = 225$E wave-1 mixed runs (top row) and for the $\lambda_0 = 0$E and $\lambda_0 = 90$E wave-2 mixed runs (second row). The wave-2 forcing is weaker here than the wave-1 forcing with $Q_S = 2$, $Q_A = 4$ used for the wave-2 run compared to $Q_S = 3$, $Q_A = 6$ used for the wave-1 run (the latter being replicated from Figure 9). Like the corresponding stronger wave-2 runs in the previous section (Figure 9), the wave-2 runs here project onto the near-surface NAM, although

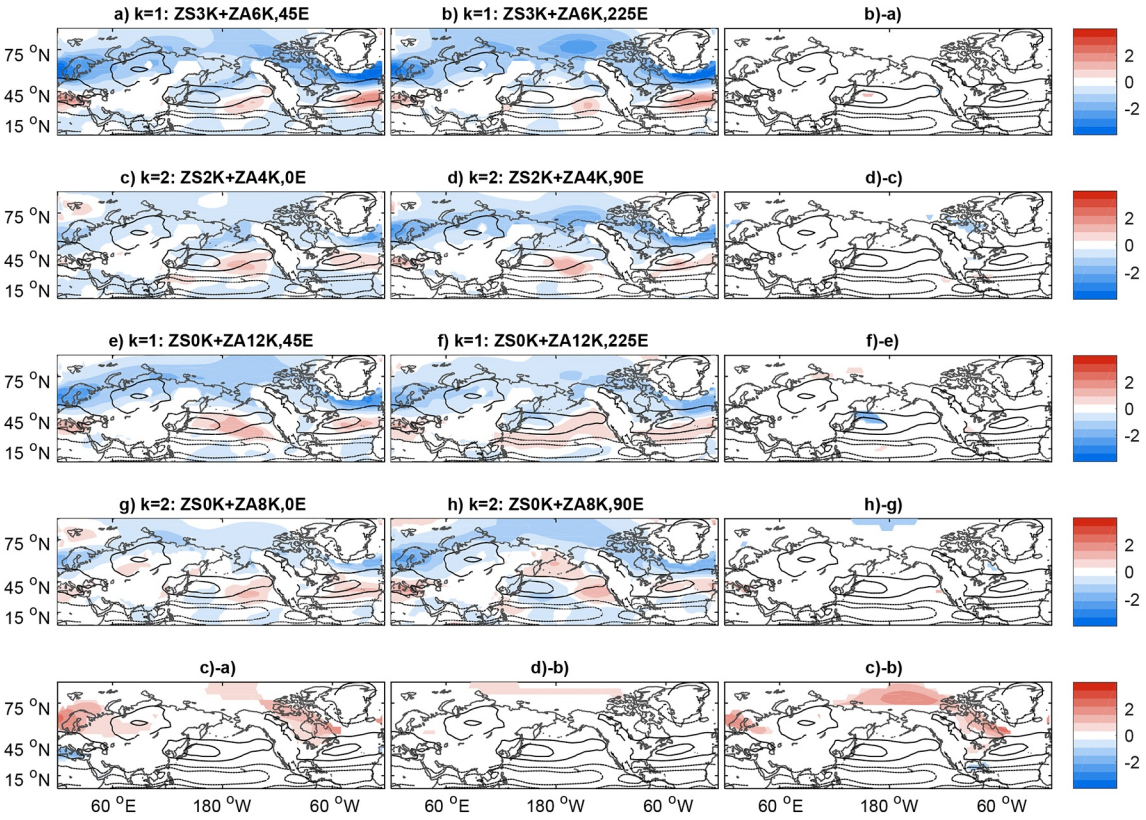

Figure 12. Same as Figure 9 except that the wave-2 PTRB experiments have been replaced with weaker mixed symmetric-asymmetric forcing ($Q_S = 2$, $Q_A = 4$) and weaker asymmetric forcing ($Q_S = 0$, $Q_A = 8$) that is two thirds of the heating magnitude for the wave-1 experiments. The wave-1 PTRB experiments are the same as in Figure 9 (i.e., first and third rows are repeated here for completeness). Wave-2 minus wave-1 differences in the final row are calculated according to the panels in this figure.

with a slightly stronger projection in the $\lambda_0 = 90$E run. This is also seen in the 970 hPa $\overline{u}$ anomalies in Figure 10b with significantly stronger $\lambda_0 = 90$E anomalies north of 70°N compared to the $\lambda_0 = 0$E anomalies (compare dashed pink and green lines). Similarly for the weaker asymmetric wave-2 runs (fourth row; here chosen to be $Q_S = 0$, $Q_A = 8$ which is approximately equivalent to the mixed forcing), a NAM projection is visible albeit with a slightly stronger projection for the $\lambda_0 = 90$E run and with a more robust projection onto the NAM over the North Atlantic/Canada. It is not clear why the weaker $\lambda_0 = 90$E mixed runs yield a significantly stronger near-surface response than the corresponding $\lambda_0 = 0$E run (dashed green and pink lines). Indeed, this difference was not present in the stronger version of this pair of runs (dashed blue and red lines in Figure 10b). This may be due to some nonlinearities associated with the phasing of the heating and the climatological stationary waves. Nevertheless, this relationship is currently under investigation and will be published elsewhere.

When comparing the mixed wave-1 and wave-2 runs (bottom row in Figure 12), there are substantial differences in the magnitude of the surface response. In particular, the wave-2 runs yield a significantly weaker tropospheric response than the wave-1 runs. This is most apparent in the $\lambda_0 = 0$E wave-2 minus $\lambda_0 = 45$E wave-1 composites (panel c–a) and in the $\lambda_0 = 0$E wave-2 minus $\lambda_0 = 225$E wave-1 composites (panel c–b). The latter is most closely associated with the locations of the control-run displacements and splits.

This weaker magnitude projection onto the near-surface NAM is perhaps expected given the weaker forcing. However, in the control-run displacements and splits, the differential stratospheric temperature anomalies still resulted in nearly indistinguishable near-surface wind anomalies in the longer-term mean (Figure 3). This therefore indicates that the tropospheric response is not solely governed by the magnitude of the stratospheric anomalies, but instead some additional factor is at work.

5. Summary and Discussion

In this study, we have examined the longer-term mean influence of displacement- and split-type SSWs on the troposphere using an idealized model. A series of transient PRTB experiments spun off from a free-running CTRL have been performed, whereby asymmetric thermal forcing was applied for a limited duration. To determine if the SSW type (be it a displacement or a split) as well as the vortex location is important for the tropospheric response, the longitude of the asymmetric warming was varied for both the wave-1 and wave-2 experiments.

In the freely evolving displacements and splits identified in the control runs, it is found that at lags of more than approximately 3–4 weeks, the tropospheric responses are indistinguishable (Figures 2 and 3). Hence, the initial asymmetry of the vortex in the aftermath of the SSW onset, does not matter for the longer-term (i.e., seasonal-timescale) response. However, at lags closer to the onset (i.e., subseasonal timescales), there are clear differences, with splits being associated with a more barotropic NAM structure that extends deep into the troposphere (also found in a comprehensive model by, e.g., Maycock & Hitchcock, 2015), whereas displacements are associated with a more gradual downward propagation over $\sim$ 10–15 days (Seviour et al., 2016). This disagrees with Mitchell et al. (2013) for instance, who found that observed split SSWs had a stronger near-surface response that lasted for longer than displacement SSWs. On the other hand, it agrees with Maycock and Hitchcock (2015) who found in a comprehensive model that displacements and splits do not exhibit salient differences unless sufficiently large samples are considered. It also agrees with Hall et al. (2021) who only found salient differences in the tropospheric temperature response at lags relatively close to their defined surface-impact date, but not at longer lags.

Two sets of PTRB runs were performed in this study. The first included both a zonally symmetric and a zonally asymmetric component to the thermal forcing (referred to as the mixed experiments throughout). These were performed to try and approximate, as closely as possible, the control-run displacements and splits that have a symmetric warming over the Polar Cap along with larger-magnitude asymmetric warming further equatorward (Figure 3). The second forcing type was zonally asymmetric (equivalent to the mixed PTRBs in terms of the overall forcing applied) which were performed in order to determine if the eddy part of the SSW structure was sufficient to yield a NAM-like tropospheric response. In both the mixed symmetric-asymmetric PTRBs and the asymmetric PTRBs, a projection onto the stratospheric and tropospheric NAM was apparent (Figures 7–10, 12) although with a stronger and more robust projection onto the tropospheric NAM over the North Atlantic/Canada than over the North Pacific. Note that the projection of the asymmetric runs onto the NAM should not be so surprising as the forcing projects onto wave-0 (i.e., yielding a net warming) courtesy of the trough removal in the forcing profile itself (Equation 5 and see Section 4.3).

Overall, in our PTRB experiments, few differences were found between the various wave-1 forced displacements and wave-2 forced splits with equal forcing (Figures 7–10). In particular, varying the longitude of the wave-1 forcing or the longitude of the wave-2 forcing does not yield significant near-surface differences. Similarly, comparing the wave-1 and wave-2 experiments also does not yield significant differences, indicating that the SSW type is somewhat unimportant for qualitatively determining the tropospheric response at long lags. These experiments therefore agree with the differences found in the control-run displacements and splits. Thus, in light of the fact that knowledge of SSWs has the potential to improve weather predictability (e.g., Rao et al., 2020; Sigmond et al., 2013), this study suggests that the SSW classification as either a split or displacement would not be sufficient to determine the magnitude of the near-surface impact at long lags.

The lack of significant differences found when varying the location of the wave-1 forcing also suggests that the observed shift in the polar vortex over the last few decades may be less important for near-surface weather than studies have suggested (Zhang et al., 2016). In particular, they found that the trend for the polar vortex to shift toward Eurasia in recent decades may have resulted in cold temperature anomalies over Eurasia and North America. However, our experiments (that are much stronger than the shifts considered in Zhang et al., 2016) indicate that a polar vortex shift by up to 180° does not result in qualitatively or quantitatively different near-surface temperature anomalies (Figure S6) on seasonal timescales. Hence, it is possible that the observed vortex shift in Zhang et al. (2016) has a negligible surface impact. Nevertheless, one should

note the different timescales considered in our two studies; our heating was imposed for 10 days whereas their study focuses on the climatological asymmetries.

An interesting feature in the control-run SSWs is that the displacements yield a weaker and warmer middle-to-upper stratospheric polar vortex than the control-run splits (Figure 4 and Figure S5). Similar results were also found in ERA-5 reanalysis, although in the lower stratosphere, the NAM indices were of similar magnitudes in both MiMA and ERA-5 (Figure 7). Despite this, the magnitude of the near-surface response was found to be indistinguishable between the two SSW types (Figures 2 and 3). Applying stronger wave-1 forcing compared to wave-2 forcing however, yielded clear differences in magnitude (Figure 12); i.e., a stronger thermal forcing, regardless of whether it is wave-1 or wave-2, elicits a stronger tropospheric response. This suggests that the magnitude of the stratospheric warming is not the only governing factor in determining the tropospheric response, but instead some other circulation anomaly related to the SSW growth and/or evolution also plays a role. Further, it suggests the importance of the lower-stratospheric anomalies as opposed to those in the middle to upper stratosphere for the tropospheric response (as suggested in, e.g., Maycock & Hitchcock, 2015).

Our results provide evidence for a coupling between the zonal-mean tropospheric circulation and the generation of the wave-2 splits. In particular, the free-running splits in the control runs show a strong barotropic signal that penetrates deep into the troposphere at the onset (Figure 2). However, despite our wave-2 PTRB experiments having a barotropic structure in the stratosphere (aside from in the lower stratosphere where the forcing linearly decreases to near the tropopause), a barotropic NAM signal is not found (Figure 8). This suggests that the barotropic NAM signal found in the freely evolving splits is likely associated with the wave-2 growth mechanism itself. Theoretical studies have shown that the growth of wave-2 in the stratosphere can occur when a stratospheric free traveling wave comes into resonance with a forced stationary wave, yielding a barotropic mode that gives rise to the split (wave-2) vortex (e.g., Esler & Scott, 2005; Plumb, 1981). Our work also suggests that the tropospheric circulation may play a role in this. Nevertheless, this is left for future work.

It is worthwhile noting that other factors (e.g., sea surface temperatures or the Madden-Julian Oscillation) may mediate the downward transmission of weak vortex events to the troposphere and explain the displacement versus split differences seen in Mitchell et al. (2013), Seviour et al. (2016) and Hall et al. (2021) as well as at short lags found here. For instance, Liu et al. (2014) found that the phase of the tropical quasi-biennial oscillation (QBO) is important for the frequency of each SSW type. In particular, during a westerly QBO phase, splits are more common whereas during an easterly phase, displacements are more prevalent. The mid-latitude temperature anomalies associated with each QBO phase may then also have an influence on the troposphere. Nevertheless, such external factors, although possible to assess using MiMA (as a QBO is spontaneously generated), are beyond the scope of this study and we have not delved into this.

Although in this paper we have focused primarily on the longer-lag response, forecasting the tropospheric response at lags closer to the SSW onset date would also provide important actionable information on subseasonal timescales given that during splits for instance, the immediate barotropic response lasts for approximately 10–14 days. Indeed, there are differences between the various PTRB experiments at shorter lags (Figure 11 and Figure S9) that may be involved in the initial downward transmission of the stratospheric signal to the troposphere and further work is needed to understand this. This study therefore shows that on subseasonal timescales, vortex morphology is important for determining the tropospheric response, whereas on seasonal timescales, it is relatively unimportant.

Data Availability Statement

The updated version of MiMA used in this study including the modified source code and example namelists to reproduce the experiments can be downloaded from https://github.com/ianpwhite/MiMA/releases/tag/MiMA-ThermalForcing-v1.0beta (with DOI: https://doi.org/10.5281/zenodo.4523199). It is expected that these modifications will also eventually be merged into the main MiMA repository which can be downloaded from https://github.com/mjucker/MiMA and is documented by Jucker and Gerber (2017), Garfinkel, White, Gerber, Jucker, and Erez (2020a), and Garfinkel, White, Gerber, and Jucker (2020b). ERA-5

reanalysis data is documented in Hersbach et al. (2020) and can be downloaded from https://www.ecmwf.int/en/forecasts/datasets/reanalysis-datasets/era5.

Acknowledgments
The authors wish to thank Ed Gerber and an anonymous reviewer whose in-depth reviews have led to a much-improved manuscript. I. P. White is also thankful for useful conversations with Chen Schwartz. The authors acknowledge the support of a European Research Council starting grant under the European Union Horizon 2020 research and innovation program (Grant 677756). J. Cohen is supported by the US National Science Foundation grant PLR-1901352. M. Jucker is supported by the ARC Centre of Excellence for Climate Extremes under Grant CE170100023 and ARC Grant FL150100035. J. Rao also acknowledges support from the National Natural Science Foundation of China (41705024).

References

Ambaum, M. H. P., & Hoskins, B. J. (2002). The NAO troposphere-stratosphere connection. *Journal of Climate*, *15*, 1969–1978. https://doi.org/10.1175/1520-0442(2002)015<1969:tntsc>2.0.co;2

Baldwin, M. P., & Dunkerton, T. J. (2001). Stratospheric harbingers of anomalous weather regimes. *Science*, *294*, 581–584. https://doi.org/10.1126/science.1063315

Baldwin, M. P., & Thompson, D. W. J. (2009). A critical comparison of stratosphere-troposphere coupling indices. *Quarterly Journal of the Royal Meteorological Society*, *135*, 1661–1672. https://doi.org/10.1002/qj.479

Butler, A. H., Seidel, D. J., Hardiman, S. C., Butchart, N., Birner, T., & Match, A. (2015). Defining sudden stratospheric warmings. *Bulletin of American Meteorological Society*, *96*, 1913–1928. https://doi.org/10.1175/bams-d-13-00173.1

Butler, A. H., Sjoberg, J. P., Seidel, D. J., & Rosenlof, K. H. (2017). A sudden stratospheric warming compendium. *Earth System Science Data*, *9*, 63–76. https://doi.org/10.5194/essd-9-63-2017

Butler, A. H., Thompson, D. W. J., & Heikes, R. (2010). The steady-state atmospheric circulation response to climate change–like thermal forcings in a simple general circulation model. *Journal of Climate*, *23*, 3474–3496. https://doi.org/10.1175/2010jcli3228.1

Charlton, A. J., O'Neill, A., Berrisford, P., & Lahoz, W. A. (2005). Can the dynamical impact of the stratosphere on the troposphere be described by large-scale adjustment to the stratospheric PV distribution? *Quarterly Journal of the Royal Meteorological Society*, *131*, 542–543. https://doi.org/10.1256/qj.03.222

Charlton, A. J., & Polvani, L. M. (2007). A new look at stratospheric sudden warmings. Part I: Climatology and modeling benchmarks. *Journal of Climate*, *20*, 449–469. https://doi.org/10.1175/jcli3996.1

Domeisen, D. I. V., Sun, L., & Chen, G. (2013). The role of synoptic eddies in the tropospheric response to stratospheric variability. *Geophysical Research Letters*, *40*, 4933–4937. https://doi.org/10.1002/grl.50943

Eliassen, A. (1951). Slow thermally or frictionally controlled meridional circulation in a circular vortex. *Astrophysica Norvegica*, *5*, 19–60.

Esler, J. G., & Scott, R. K. (2005). Excitation of transient rossby waves on the stratospheric polar vortex and the barotropic sudden warming. *Journal of the Atmospheric Sciences*, *62*, 3661–3682. https://doi.org/10.1175/jas3557.1

Garfinkel, C. I., White, I. P., Gerber, E. P., & Jucker, M. (2020b). The impact of SST biases in the tropical east pacific and Agulhas current region on atmospheric stationary waves in the southern hemisphere. *Journal of Climate*, *33*, 9351–9374. https://doi.org/10.1175/JCLI-D-20-0195.1

Garfinkel, C. I., White, I. P., Gerber, E. P., Jucker, M., & Erez, M. (2020a). The building blocks of northern hemisphere wintertime stationary waves. *Journal of Climate*, *33*(13), 5611–5633. https://doi.org/10.1175/jcli-d-19-0181.1

Gerber, E. P., Voronin, S., & Polvani, L. P. (2008). Testing the annular mode autocorrelation time scale in simple atmospheric general circulation models. *Monthly Weather Review*, *136*, 1523–1536. https://doi.org/10.1175/2007mwr2211.1

Hall, R. J., Mitchell, D. M., Seviour, W. J., & Wright, C. J. (2021). Tracking the stratosphere-to-surface impact of sudden stratospheric warmings. *Journal of Geophysical Research*, *126*. https://doi.org/10.1029/2020JD033881

Hersbach, H., Bell, B., Berrisford, P., Hirahara, S., Horanyi, A., Munoz-Sabater, J., & Thepaut, J.-N. (2020). The era5 global reanalysis. *Quarterly Journal of the Royal Meteorological Society*, *146*(730), 1999–2049. https://doi.org/10.1002/qj.3803

Hitchcock, P., & Simpson, I. R. (2014). The downward influence of stratospheric sudden warmings. *Journal of the Atmospheric Sciences*, *71*, 3856–3876. https://doi.org/10.1175/jas-d-14-0012.1

Jucker, M. (2016). Are sudden stratospheric warmings generic? Insights from an idealized gcm. *Journal of Climate*, *73*, 5061–5080. https://doi.org/10.1175/jas-d-15-0353.1

Jucker, M., & Gerber, E. P. (2017). Untangling the annual cycle of the tropical tropopause layer with an idealized moist model. *Journal of Climate*, *30*, 7339–7358. https://doi.org/10.1175/jcli-d-17-0127.1

Karpechko, A. Y., Hitchcock, P., Peters, D. H. W., & Schneidereit, A. (2017). Predictability of downward propagation of major sudden stratospheric warmings. *Quarterly Journal of the Royal Meteorological Society*, *143*, 1459–1470. https://doi.org/10.1002/qj.3017

Kushner, P. J., & Polvani, L. M. (2004). Stratosphere-troposphere coupling in a relatively simple AGCM: The role of eddies. *Journal of Climate*, *17*, 629–639. https://doi.org/10.1175/1520-0442(2004)017<0629:sciars>2.0.co;2

Liu, C., Tian, B., Li, K.-F., Manney, G. L., Livesey, N. J., Yung, Y. L., & Waliser, D. E. (2014). Northern hemisphere mid-winter vortex-displacement and vortex-split stratospheric sudden warmings: Influence of the Madden-Julian oscillation and Quasi-Biennial Oscillation. *Journal of Geophysical Research - D: Atmospheres*, *119*(22), 12599–12620. https://doi.org/10.1002/2014jd021876

Maycock, A. C., & Hitchcock, P. (2015). Do split and displacement sudden stratospheric warmings have different annular mode signatures? *Geophysical Research Letters*, *42*, 10943–10951. https://doi.org/10.1002/2015gl066754

Mitchell, D., Gray, L. J., Anstey, J. A., Baldwin, M. P., & Charlton-Perez, A. J. (2013). The influence of stratospheric vortex displacements and splits on surface climate. *Journal of Climate*, *26*, 2668–2682. https://doi.org/10.1175/jcli-d-12-00030.1

O'Callaghan, A., Joshi, M., Stevens, D., & Mitchell, D. (2014). The effects of different sudden stratospheric warming types on the ocean. *Geophysical Research Letters*, *41*, 7739–7745. https://doi.org/10.1002/2014GL062179

Plumb, R. A. (1981). Instability of the distorted polar night vortex: A theory of stratospheric warmings. *Journal of the Atmospheric Sciences*, *38*, 2514–2531. https://doi.org/10.1175/1520-0469(1981)038<2514:iotdpn>2.0.co;2

Polvani, L. M., & Kushner, P. (2002). Tropospheric response to stratospheric perturbations in a relatively simple general circulation model. *Geophysical Research Letters*, *29*(7). https://doi.org/10.1029/2001gl014284

Rao, J., Garfinkel, C. I., & White, I. P. (2020). Predicting the downward and surface influence of the February 2018 and January 2019 sudden stratospheric warming events in subseasonal to seasonal (s2s) models. *Journal of Geophysical Research*, *125*. https://doi.org/10.1029/2019jd031919

Runde, T., Dameris, M., Garny, H., & Kinnison, D. E. (2016). Classification of stratospheric extreme events according to their downward propagation to the troposphere. *Geophysical Research Letters*, *43*, 6665–6672. https://doi.org/10.1002/2016gl069569

Seviour, W. J. M., Gray, L. J., & Mitchell, D. M. (2016). Stratospheric polar vortex splits and displacements in the high-top cmip5 climate models. *Journal of Geophysical Research*, *121*, 1400–1413. https://doi.org/10.1002/2015jd024178

Seviour, W. J. M., Mitchell, D. M., & Gray, L. J. (2013). A practical method to identify displaced and split stratospheric polar vortex events. *Geophysical Research Letters*, *40*, 5268–5273. https://doi.org/10.1002/grl.50927

Sigmond, M., Scinocca, J. F., Kharin, V. V., & Shepherd, T. G. (2013). Enhanced seasonal forecast skill following stratospheric sudden warmings. *Nature Geoscience*, *6*, 98–102. https://doi.org/10.1038/ngeo1698

Smy, L. A., & Scott, R. K. (2009). The influence of stratospheric potential vorticity on baroclinic instability. *Quarterly Journal of the Royal Meteorological Society*, *135*, 1673–1683. https://doi.org/10.1002/qj.484

Song, Y., & Robinson, W. (2004). Dynamical mechanisms for stratospheric influences on the troposphere. *Journal of the Atmospheric Sciences*, *61*, 1711–1725. https://doi.org/10.1175/1520-0469(2004)061<1711:dmfsio>2.0.co;2

White, I. P., Garfinkel, C. I., Gerber, E. P., Jucker, M., Aquila, V. A., & Oman, L. D. (2019). The downward influence of sudden stratospheric warmings: Association with tropospheric precursors. *Journal of Climate*, *32*, 85–108. https://doi.org/10.1175/jcli-d-18-0053.1

White, I. P., Garfinkel, C. I., Gerber, E. P., Jucker, M., Hitchcock, P., & Rao, J. (2020). The generic nature of the tropospheric response to sudden stratospheric warmings. *Journal of Climate*, *33*(13), 5589–5610. https://doi.org/10.1175/jcli-d-19-0697.1

Zhang, J., Tian, W., Chipperfield, M. P., Xie, F., & Huang, J. (2016). Persistent shift of the arctic polar vortex toward the eurasian continent in recent decades. *Nature Climate Change*, *6*, 1094–1099. https://doi.org/10.1038/nclimate3136